Flexural phonons and thermal transport in multilayer graphene and graphite

L. Lindsay,[1,2] D. A. Broido,[1,*] and Natalio Mingo[3,4]

[1]*Department of Physics, Boston College, Chestnut Hill, Massachusetts 02467, USA*

[2]*Department of Physics, Computer Science, and Engineering, Christopher Newport University, Newport News, Virginia 23606, USA*

[3]*CEA-Grenoble, 17 Rue des Martyrs, Grenoble 38000, France*

[4]*Department of Electrical Engineering, University of California, Santa Cruz, California 95064, USA*

(Received 25 May 2011; published 29 June 2011)

We present a theory for the lattice thermal conductivity κ_L of multilayer graphene (MLG) and graphite, which is based on an exact numerical solution of the Boltzmann equation for phonons. Dominant contributions to κ_L from out-of-plane or flexural phonons are found, which is consistent with previous findings for single-layer graphene (SLG). However, the interaction between graphene layers in MLG and graphite breaks a selection rule on phonon-phonon scattering, causing their κ_Ls to be much lower than that of SLG. C^{13} isotopes are shown to be an important scattering mechanism, accounting for an ~15% additional drop in the κ_L of these systems. We demonstrate that the κ_L values converge to that of graphite after only about five layers, a consequence of weak interlayer coupling. These findings are qualitatively consistent with recent measurements of κ_L for MLG.

DOI: 10.1103/PhysRevB.83.235428 PACS number(s): 63.22.Rc, 63.20.kg, 65.80.Ck, 66.70.−f

I. INTRODUCTION

Graphene and graphite, along with other carbon-based structures such as diamond and carbon nanotubes, have among the highest thermal conductivities of any known materials. In these systems, heat is carried by phonons, and around room temperature, the lattice thermal conductivity κ_L is limited by phonon-phonon interactions caused by the anharmonicity of the interatomic potential.[1] In diamond, the strong covalent bonding and light carbon atoms produce large phonon velocities and an extremely restricted phase space for phonon-phonon scattering, causing large amounts of heat to be transported by the two transverse acoustic (*TA*) and one longitudinal acoustic (*LA*) phonon branches.[2,3] One might expect graphene to be the two-dimensional (2D) analogue to this, with the majority of heat carried by one *TA* and one *LA* branch. However, along with these modes that vibrate in the plane of the graphene layer, there are also out-of-plane vibrations—the so-called flexural modes. The lowest flexural phonon branch (labeled *ZA*) exhibits an unusual quadratic dispersion $\omega \sim q^2$, making the group velocity vanish as $q \to 0$. As a result, it was natural to assume that the flexural modes carry little heat.[4–8]

Recently, we showed that the opposite is true[9,10]: The reflection symmetry about the graphene plane leads to a selection rule that strongly inhibits phonon-phonon scattering. This, combined with their large thermal population, causes the *ZA* phonons to provide the dominant contribution to κ_L, one much greater than the in-plane contributions combined. This surprising result is consistent with recent thermal transport measurements on graphene structures.[9,11–13]

Graphene is the building block for graphite, so it is natural to ask, (1) How are the magnitudes of κ_{graphene} and κ_{graphite} related? and (2) How does κ_{graphene} evolve into κ_{graphite} with an increasing number of graphene layers? Experimentally, these questions have not been conclusively answered yet. The measured room temperature values of κ_L for graphene are in the range $\kappa_{\text{graphene}} \approx 600$–$5800$ $\text{Wm}^{-1}\text{K}^{-1}$,[14–18] whereas $\kappa_{\text{graphite}} \approx 2000$ $\text{Wm}^{-1}\text{K}^{-1}$.[19] Recent measurements of κ_L for multilayer graphene (MLG) show that κ_L decreases with an increasing layer number N but that values for $N = 4$ and $N \approx 8$ lie below that of κ_{graphite}.[20]

In this paper, we present a theory of thermal transport and κ_L for MLG and graphite in the context of our new picture of phonon transport, where the flexural mode contributions dominate κ_L. We show that the interaction between graphene layers breaks the graphene selection rule on phonon-phonon scattering and leads to a substantial reduction in the flexural mode contributions to κ_L, which in turn decreases monotonically with an increasing number of graphene layers. This mandates that $\kappa_{\text{graphene}} > \kappa_{\text{graphite}}$. Furthermore, we find that with increasing layer number, the graphite limit is rapidly reached: κ_L evolves from κ_{graphene} to κ_{graphite} within only about five layers. These findings are in qualitative agreement with the recently measured trends for κ_L in MLG.[20]

II. INTERLAYER COUPLING

Layered graphene systems have strong in-plane covalent bonding of carbon atoms and weak Van der Waals coupling between planes. An optimized Tersoff empirical interatomic potential,[21,22] which gives improved fits to the acoustic phonon dispersions in graphite, is used to describe the in-plane bonding. A Lennard-Jones potential is used for the interplanar bonding,

$$V_{LJ}(r_{ij}) = 4\varepsilon[(\sigma/r_{ij})^{12} - (\sigma/r_{ij})^{6}], \tag{1}$$

where the parameters ε and σ are adjusted to best fit the c-axis phonon dispersion for graphite[23] and r_{ij} is the distance between atoms i and j. The values $\varepsilon = 4.6$ meV and $\sigma = 0.3276$ nm give a separation between carbon planes of $\delta = 0.335$ nm, which is in agreement with the measured value.[19] We include only coupling between adjacent carbon planes.

The phonon dispersions for N-layered graphene (graphite) are calculated by diagonalizing the dynamical matrices

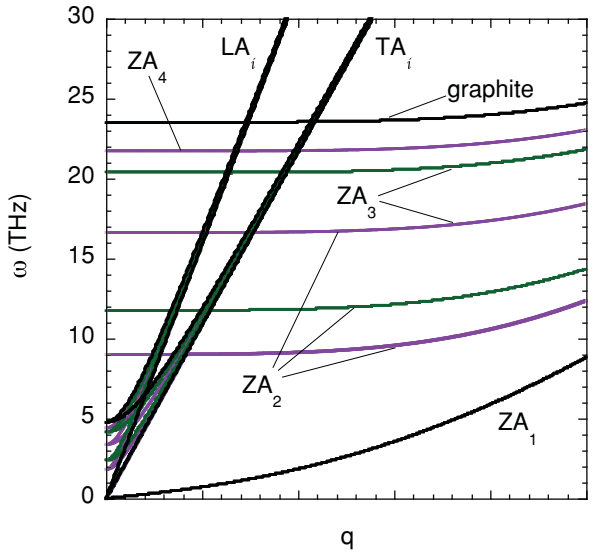

FIG. 1. (Color online) A portion of the low-frequency part of the phonon dispersion showing the TA_i, LA_i, and ZA_i branches. Purple (dark gray) curves are for both $N = 2$ and $N = 4$; green (light gray) curves are for $N = 3$.

$$D^{\kappa\kappa'}_{\alpha\beta}(\mathbf{q}) = \frac{1}{M}\sum_{l'}\Phi_{\alpha\beta}(0\kappa,l'\kappa')e^{i\mathbf{q}\cdot\mathbf{R}_{l'}} \tag{2}$$

to obtain the phonon frequencies ω_λ for each 2D or three-dimensional (3D) wavevector $\mathbf{q}$ on a grid throughout the Brillouin zone, where $\lambda = (\mathbf{q}, j)$ and j labels the phonon branch. In Eq. (2), $l\kappa$ designates the κth atom in the lth unit cell whose lattice vector is $\mathbf{R}_l$, M is the mass of the carbon atoms, and α and β are Cartesian components. Also in (2), $\Phi_{\alpha\beta}(0\kappa,l'\kappa')$ are second-order interatomic force constants (IFCs), which are determined by the combined Tersoff and Lennard-Jones potentials. For N-layer graphene, the phonon frequencies at each 2D $\mathbf{q}$ point considered are obtained by numerically diagonalizing the $6N \times 6N$ dynamical matrix using a standard LAPACK (Linear Algebra PACKage) routine for Hermitian matrices. For graphite, a corresponding 12×12 dynamical matrix is diagnonalized using the same routine for each 3D $\mathbf{q}$ point considered.

Our focus is on the low-frequency part of the phonon spectrum, a portion of which is shown in Fig. 1, because these branches carry most of the heat and only in this range is the phonon dispersion different from that in graphene. N-layered graphene and graphite each have three acoustic branches with phonon frequencies $\omega_\lambda \to 0$ as phonon wavevector $\mathbf{q} \to 0$. In-plane transverse and longitudinal branches (TA_1 and LA_1) have linear dispersion near the Brillouin zone center, whereas an out-of-plane, flexural branch (ZA_1) has quadratic dispersion, except for very small $\mathbf{q}$.[24,25] For the multilayers ($N > 1$), the weak interlayer coupling produces $N - 1$ low-lying optic phonon branches for each acoustic branch, which we label $TA_{i>1}$, $LA_{i>1}$, and $ZA_{i>1}$. The $TA_{i>1}$ and $LA_{i>1}$ branches deviate from TA_1 and LA_1 only very near the Γ-point, whereas the flexural branches $ZA_{i>1}$ deviate significantly from the ZA_1 branch throughout much of the Brillouin zone.

III. BREAKING OF SELECTION RULE

The intrinsic resistance to heat flow in graphene-based structures is limited by three-phonon scattering, which dominates κ_L around and above room temperature.[1] The phase space for this scattering is defined from all three-phonon processes satisfying the conservation of energy and momentum: $\omega_j(\mathbf{q}) \pm \omega_{j'}(\mathbf{q}') = \omega_{j''}(\mathbf{q}'')$ and $\mathbf{q} \pm \mathbf{q}' = \mathbf{q}'' + \mathbf{K}$, where $\mathbf{K}$ is a reciprocal lattice vector, which is zero for normal processes and nonzero for umklapp processes. The strength of a three-phonon scattering process is governed by the matrix elements:[10]

$$\Phi_{\lambda\lambda'\lambda''} = \sum_{\kappa}\sum_{l'\kappa'}\sum_{l''\kappa''}\sum_{\alpha\beta\gamma}\Phi_{\alpha\beta\gamma}\left(0\kappa,l'\kappa',l''\kappa''\right) \times e^{\lambda}_{\alpha\kappa}e^{\lambda'}_{\beta\kappa'}e^{\lambda''}_{\gamma\kappa''}e^{i\mathbf{q}'\cdot\mathbf{R}_{l'}}e^{i\mathbf{q}''\cdot\mathbf{R}_{l''}}. \tag{3}$$

The $\Phi_{\alpha\beta\gamma}(0\kappa,l'\kappa',l''\kappa'')$ are third-order anharmonic IFCs, and the $e^{\lambda}_{\alpha\kappa}$ are phonon eigenvectors. We showed previously[9,10] that reflection symmetry about a single graphene sheet (or any 2D crystal) requires that the nth order anharmonic IFCs vanish: $\Phi_{\alpha_1\ldots\alpha_n}(l_1\kappa_1;\ldots;l_n\kappa_n) = 0$, when the number of out-of-plane components in the string $\alpha_1\ldots\alpha_n$ is odd. This leads to a selection rule that forbids any n-phonon scattering process involving an odd number of out-of-plane phonons. For three-phonon scattering, the matrix element, Eq. (3), vanishes for processes such as $ZA + ZA \leftrightarrow ZA$ and $ZA + TA \leftrightarrow LA$, eliminating $\sim$60% of the scattering phase space for ZA phonons and significantly increasing their intrinsic scattering times. This, combined with their large thermal populations, is why the ZA phonons provide the dominant contribution to κ_L in graphene.

In MLG and graphite, reflection symmetry applied to the nth order *interlayer* IFCs gives

$$\Phi_{\alpha_1\ldots\alpha_n}(l'_1\kappa'_1;\ldots l'_i\kappa'_i;\ldots;l'_n\kappa'_n) = (-1)^m\Phi_{\alpha_1\ldots\alpha_n}(l_1\kappa_1;\ldots l_i\kappa_i\ldots;l_n\kappa_n), \tag{4}$$

where m is the number of out-of-plane components in $\alpha_1\ldots\alpha_n$ and $l'_i\kappa'_i$ designates the atom into which $l_i\kappa_i$ is mapped across the reflection plane (chosen to be in the middle of the structure). Because at least one $l_i\kappa_i$ resides in a different layer, Eq. (4) simply reduces the number of distinct IFCs but does not require any to vanish. As a result, the graphene selection rule does not hold, and the previously forbidden scattering becomes allowed, providing additional resistance to phonon flow.

IV. THERMAL TRANSPORT THEORY

We calculate κ_L for N-layer graphene and graphite using an exact numerical solution to the phonon Boltzmann transport equation (BTE), previously described elsewhere for single-walled carbon nanotubes (SWCNTs)[26,27] and graphene.[9,10] The solution of the BTE gives the nonequilibrium phonon distribution functions resulting from the temperature gradient applied across the graphene structure. These functions are directly related to τ_λ, the phonon lifetimes in mode λ. Here, the BTE is cast in terms of a set of coupled equations for these τ_λ:

$$\tau_\lambda = \tau^0_\lambda + \tau^0_\lambda\Delta_\lambda. \tag{5}$$

In Eq. (5),

$$\Delta_\lambda = \sum_{\lambda'\lambda''}{}^{(+)} \Gamma^{(+)}_{\lambda\lambda'\lambda''}(\xi_{\lambda\lambda''}\tau_{\lambda''} - \xi_{\lambda\lambda'}\tau_{\lambda'}) + \frac{1}{2}\sum_{\lambda'\lambda''}{}^{(-)} \Gamma^{(-)}_{\lambda\lambda'\lambda''}(\xi_{\lambda\lambda''}\tau_{\lambda''} + \xi_{\lambda\lambda'}\tau_{\lambda'}), \quad (6)$$

where $\xi_{\lambda\lambda'} = v_{\lambda'}\omega_{\lambda'}/v_\lambda\omega_\lambda$, with v_λ being the velocity component along the transport direction, and the sums are over the phase space for three-phonon scattering, satisfying energy and momentum conservation conditions, mentioned before Eq. (3). The $\Gamma^{(\pm)}_{\lambda\lambda'\lambda''}$ are the intrinsic anharmonic scattering rates

$$\Gamma^{(\pm)}_{\lambda\lambda'\lambda''} = \frac{\hbar\pi}{4M^3}\left\{\begin{matrix} n^0_{\lambda'} - n^0_{\lambda''} \\ n^0_{\lambda'} + n^0_{\lambda''} + 1 \end{matrix}\right\} |\Phi^{(\pm)}_{\lambda,\pm\lambda',-\lambda''}|^2 \times \delta(\omega_\lambda \pm \omega_{\lambda'} - \omega_{\lambda''}), \quad (7)$$

with n^0_λ being the Bose factor and $-\lambda \Rightarrow (-\mathbf{q}, j)$. The τ^0_λ in Eq. (5) are the lifetimes within the relaxation time approximation solution of the BTE:

$$1/\tau^0_\lambda \equiv \sum\nolimits_{(+)} \Gamma^{(+)}_{\lambda\lambda'\lambda''} + 1/2 \sum\nolimits_{(-)} \Gamma^{(-)}_{\lambda\lambda'\lambda''} + 1/\tau^{bs}_\lambda. \quad (8)$$

τ^0_λ is directly determined by the intrinsic anharmonic scattering rates and by any other extrinsic scattering processes. In this paper, we include boundary scattering of phonons along the transport direction taken to be of length L. The choice of $\tau^{bs}_\lambda = L/2|v_\lambda|$ gives the correct limiting values of the thermal conductivity in the ballistic ($L \to 0$) and diffusive ($L \to \infty$) limits.[28]

The BTE in Eq. (5) is solved using an iterative scheme. To begin this process, a grid of points is defined throughout the Brillouin zone. For each λ, the phase space of λ' and λ'' values is found numerically using a root-finding algorithm, and the anharmonic scattering rates are calculated from Eq. (7). This allows determination of τ^0_λ from Eq. (8). $\tau^{(0)}_\lambda = \tau^0_\lambda$ is used then in Eq. (6) for the zeroth iteration. Plugging this into Eq. (5) yields $\tau^{(1)}_\lambda$. The iteration scheme is continued until the calculated κ_L from Eq. (9) (given later) differs negligibly on successive iterations. For MLG, the graphene BTE solution[9,10] is generalized to include interlayer coupling, with a unit cell size of $2N$. For graphite, the unit cell contains four atoms and a 3D $\mathbf{q}$-space must be used. Our approach automatically includes normal and umklapp processes. This is particularly important for graphene-based systems, where quadratic ZA dispersion makes normal scattering of low-frequency phonons far more prevalent than is the case for systems that have only linear acoustic branches.[10]

The BTE solution yields the nonequilibrium distribution functions from which the phonon scattering times τ_λ are obtained. The κ_L for each system is determined from

$$\kappa_L = \begin{cases} \frac{1}{(2\pi)^2(N\delta)} \sum_j \int \left(\partial n^0_\lambda/\partial T\right)\hbar\omega_\lambda v^2_\lambda \tau_\lambda d\,\mathbf{q} & N-\text{layer graphene} \\ \frac{1}{(2\pi)^3} \sum_j \int \left(\partial n^0_\lambda/\partial T\right)\hbar\omega_\lambda v^2_\lambda \tau_\lambda d\mathbf{q} & \text{graphite} \end{cases} \quad (9)$$

In the upper and lower expressions, the integral is 2D and 3D, respectively.

V. RESULTS AND DISCUSSION

In all calculations, the thermal transport is in the $\Gamma \to M$ direction, and the lateral dimension has been taken to be infinite.[29] The breaking of the graphene selection rule for the multilayers causes the phase space for three-phonon scattering to become very large and to increase rapidly with N. This presents a significant numerical challenge that has limited our consideration to $N \leqslant 5$. Figure 2 shows κ_L vs N (black circles) scaled by the calculated value: $\kappa_{\text{graphene}} \approx 3500\ \text{Wm}^{-1}\text{K}^{-1}$ for sample length $L = 10\ \mu$m at temperature $T = 300$K (the typical sample lengths have L in the range of 1–10 μm[14–16,18,20]). Also shown are the scaled per-branch-type contributions to the total κ_L for each system, κ_{ZA}, κ_{TA}, and κ_{LA} (red, green, and blue circles), where $\kappa_{ZA} = \sum_{i=1}^{N}\kappa_{ZA_i}$, etc. The contribution from high-lying optic branches is small and not shown. For graphite, the enormous three-phonon phase space has precluded a fully convergent result. Nevertheless, from the trend values obtained from the BTE solution for increasingly fine $\mathbf{q}$-point grids, we have obtained an approximate thermal conductivity κ_{graphite}, which we estimate to be within ~10% of the converged value (dashed black line). The dashed red, green, and blue lines correspond to the per-branch-type values in graphite.

Over the full range of N, the ZA contribution is far larger than that from TA or LA: the thermal transport is dominated by the low-frequency out-of-plane ZA_i phonons, consistent with our previous findings for graphene[9,10] and large-diameter SWCNTs.[27] Furthermore, κ_{TA} and κ_{LA} hardly vary with N, whereas κ_{ZA} decreases by almost 50% in going from $N = 1$ to $N = 5$. The substantial reduction of κ_L for MLG occurs in part because of the raised frequencies of the $ZA_{i>1}$ phonon modes and the stiffening of the low-frequency ZA dispersion.[24,25] However, *the primary reason for the drop in κ_L is the breaking of the graphene selection rule*. To demonstrate this, we note that $\kappa_{\text{bilayer}} = 0.73\kappa_{\text{graphene}}$.[30] Recalculating κ_{bilayer} with all three-phonon processes that violate the graphene selection rule artificially removed increases the ratio to $\kappa_{\text{bilayer}} = 0.92\kappa_{\text{graphene}}$. This shows that the selection rule violation accounts for ~70% of the drop in κ_L.

About 80% of the total decrease in κ_L occurs in going from the graphene to the bilayer. By $N = 5$, κ_L has essentially saturated to ~65% of κ_{graphene} (κ_L drops by only 2% in going from $N = 4$ to $N = 5$). Thus, κ_L evolves from graphene to graphite within the first approximately five layers. The black dotted curve is a guide to the eye that highlights this behavior. This rapid transition occurs because the interlayer interactions

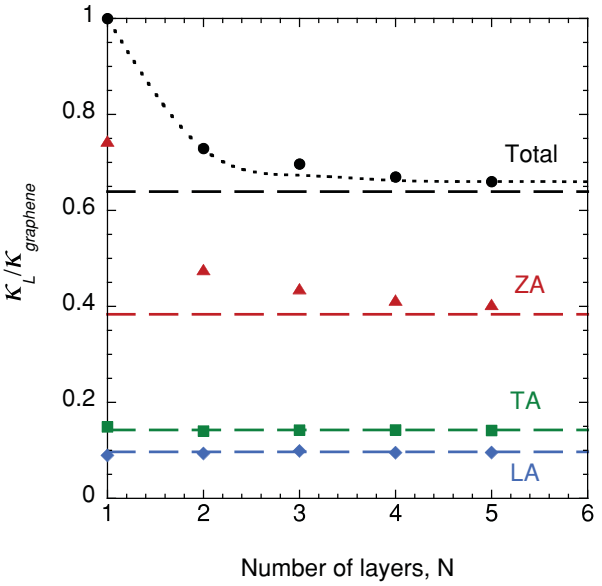

FIG. 2. (Color online) Calculated κ_L for MLG vs layer number N for $N = 1$–5 (black circles). Also shown are the per-branch contributions for *ZA* (red triangles), *TA* (green squares), and *LA* (blue diamonds) branches. The corresponding calculatedgraphite values are shown by the horizontal lines.

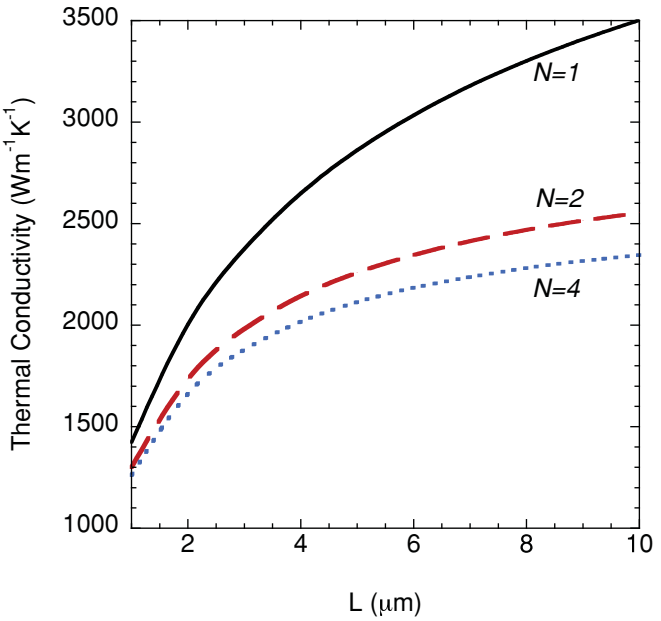

FIG. 3. (Color online) Calculated κ_L for graphene ($N = 1$, solid black curve), bilayer graphene ($N = 2$, dashed red curve), and quadrilayer graphene ($N = 4$, dotted blue curve) as a function of sample length L for $T = 300$K. On this scale, the $N = 3$ and $N = 5$ curves cannot be distinguished from that for $N = 4$.

are weak and short ranged, causing a given graphene layer to only feel adjacent layers.

Figure 3 shows κ_L for $N = 1, 2$, and 4 as a function of L in the range $L = 1$–10 μm. For small L, transport is ballistic and κ_L is independent of N. The observed stronger L dependence for graphene arises from the large intrinsic scattering times τ_λ for many *ZA* phonons, which allows them to travel ballistically across the sample. This is a consequence of the graphene selection rule. The *TA* and *LA* phonon contributions (not shown) have little L dependence over this range,[10] reflective of diffusive transport arising from their smaller τ_λ. For MLG, the L dependence of κ_L becomes noticeably weaker, because the breaking of the graphene selection rule provides new scattering channels for *ZA* phonons, which gives them a more diffusive behavior.

In real graphene and graphite samples, phonon scattering by isotopic impurities lowers κ_L. Similar to the derivation for cubic crystals,[31] we can show that the graphene isotopic impurity scattering rates are $1/\tau_F^{\rm iso}(\omega) = \pi g S_0 \omega^2 D_F(\omega)/2$ and $1/\tau_{\rm in}^{\rm iso}(\omega) = \pi g S_0 \omega^2 D_{\rm in}(\omega)/4$, where g is the mass variance parameter (for carbon crystals, $g = 7.54 \times 10^{-5}$ for 1.1% C^{13} impurities in C^{12}, as shown in Ref. 2), S_0 is the area per carbon atom, and $D_F(\omega)$ and $D_{\rm in}(\omega)$ are the densities of states per unit area for flexural (F) and in-plane (in) phonons. Using these expressions, we find a $10 \sim 15\%$ reduction in the graphene and MLG κ_L shown in Figs. 2 and 3.

Our calculated κ_L for graphene is in reasonable agreement with measured values. Including the isotope scattering, we find $\kappa_L \approx 2600$ $\mathrm{Wm^{-1}K^{-1}}$ for $L = 5$ μm, which is just below the range of measured values for similar length samples from Refs. 14 and 15 ($\sim$3000–5800 $\mathrm{Wm^{-1}K^{-1}}$) and within the range found in Refs. 16 and 18 ($\sim$1500–3500 $\mathrm{Wm^{-1}K^{-1}}$). Large uncertainties[18] have thus far precluded experimental identification of a length dependence such as indicated in Fig. 3. For MLG, a large decrease in κ_L is observed with an increasing number of layers.[20] This is qualitatively consistent with our theory, which predicts that the large drop comes from suppression of flexural phonon contributions. Conceptually, the out-of-plane vibrations should be more strongly affected by interlayer interactions than the in-plane modes, because the latter's vibrations are parallel to the layers. Finally, our finding that κ_L saturates to the graphite value after only about five layers is qualitatively consistent with the measured saturation of about eight layers.[20]

VI. CONCLUSIONS

A theory of κ_L in MLG and graphite has been developed that highlights the dominant contributions of the flexural phonons. We have shown that the interlayer coupling breaks the graphene selection rule, leading to strong suppression of the flexural phonon contributions to κ_L and correspondingly large reductions in κ_L itself, establishing that $\kappa_{\rm graphene} > \kappa_{\rm graphite}$. The κ_L decreases monotonically with an increasing number of layers and lies significantly below the graphene κ_L. Finally, κ_L converges to the graphite value after only about five layers, reflecting the very limited range of the interlayer interactions. These findings are in reasonable agreement with a number of recent experiments on SLG and MLG.

ACKNOWLEDGMENTS

D.A.B. acknowledges support from the National Science Foundation under grant number 1066634. N.M. acknowledges support from the Fondation Nanosciences and Agence Nationale de la Recherche.

*broido@bc.edu.

[1] J. M. Ziman, *Electrons and Phonons* (Oxford University Press, London, 1960).

[2] D. G. Onn, A. Witek, Y. Z. Qiu, T. R. Anthony, and W. F. Banholzer, Phys. Rev. Lett. **68**, 2806 (1992).

[3] A. Ward, D. A. Broido, D. A. Stewart, and G. Deinzer, Phys. Rev. B **80**, 125203 (2009).

[4] P. G. Klemens, J. Wide Bandgap Mater. **7**, 332 (2000).

[5] P. G. Klemens, Int. J. Thermophys. **22**, 265 (2001).

[6] D. L. Nika, S. Ghosh, E. P. Pokatilov, and A. A. Balandin, Appl. Phys. Lett. **94**, 203103 (2009).

[7] D. L. Nika, E. P. Pokatilov, A. S. Askerov, and A. A. Balandin, Phys. Rev. B **79**, 155413 (2009).

[8] B. D. Kong, S. Paul, M. B. Nardelli, and K. W. Kim, Phys. Rev. B **80**, 033406 (2009).

[9] J. H. Seol, I. Jo, A. L. Moore, L. Lindsay, Z. H. Aitken, M. T. Pettes, X. Li, Z. Yao, R. Huang, D. A. Broido, N. Mingo, R. S. Ruoff, and L. Shi, Science **328**, 213 (2010).

[10] L. Lindsay, D. A. Broido, and N. Mingo, Phys. Rev. B **82**, 115427 (2010).

[11] W. Jang, Z. Chen, W. Bao, C. N. Lau, and C. Dames, Nano Lett. **10**, 3909 (2010).

[12] Z. Wang, R. Xie, T. C. Bui, D. Liu, X. Ni, B. Li, and J. T. L. Thong, Nano Lett. **11**, 113 (2011).

[13] M. T. Pettes, I. Jo, Z. Yao, and L. Shi, Nano Lett. **11**, 1195 (2011).

[14] A. A. Balandin, S. Ghosh, W. Bao, I. Calizo, D. Teweldebrhan, F. Miao, and C. N. Lau, Nano Lett. **8**, 902 (2008).

[15] S. Ghosh, I. Calizo, D. Teweldebrhan, E. P. Pokatilov, D. L. Nika, A. A. Balandin, W. Bao, F. Miao, and C. N. Lau, Appl. Phys. Lett. **92**, 151911 (2008).

[16] W. Cai, A. L. Moore, Y. Zhu, X. Li, S. Chen, L. Shi, and R. S. Ruoff, Nano Lett. **10**, 1645 (2010).

[17] G. Faugeras, B. Faugeras, M. Orlita, M. Potemski, R. R. Nair, and A. K. Geim, ACS Nano **4**, 1889 (2010).

[18] S. Chen, A. L. Moore, W. Cai, J. W. Suk, J. An, C. Mishra, C. Amos, C. W. Magnuson, J. Kang, L. Shi, and R. Ruoff, ACS Nano **5**, 321 (2011).

[19] G. A. Slack, Phys. Rev. **127**, 694 (1962).

[20] S. Ghosh, W. Bao, D. L. Nika, S. Subrina, E. P. Pokatilov, C. N. Lau, and A. A. Balandin, Nat. Mater. **9**, 555 (2010).

[21] J. Tersoff, Phys. Rev. Lett. **61**, 2879 (1988).

[22] L. Lindsay and D. A. Broido, Phys. Rev. B **81**, 205441 (2010).

[23] R. Nicklow, N. Wakabayashi, and H. G. Smith, Phys. Rev. B **5**, 4951 (1972).

[24] For MLG, we find $\omega_{ZA}(q \to 0) \sim q^x$, with $2 > x > 1$ and x decreasing as N increases from 2 to 5. We confirm numerically that in graphite $\omega_{ZA}(q \to 0) \sim q$, as pointed out in Ref. 25.

[25] A. H. Castro Neto, F. Guinea, N. M. R. Peres, K. S. Novoselov, and A. K. Geim, Rev. mod. Phys. **81**, 109 (2009).

[26] L. Lindsay, D. A. Broido, and N. Mingo, Phys. Rev. B **80**, 125407 (2009).

[27] L. Lindsay, D. A. Broido, and N. Mingo, Phys. Rev. B **82**, 161402(R) (2010).

[28] N. Mingo and D. A. Broido, Nano Lett. **5**, 1221 (2005).

[29] Inclusion of lateral boundary scattering has only a modest effect on κ_L. Analytical considerations indicate that such scattering in 2D layers is weaker than in nanowires (Z. Wang and N. Mingo, unpublished).

[30] This large drop contrasts with Ref. 8, which found $\kappa_{\text{bilayer}} \approx \kappa_{\text{graphene}}$. Ref. 8 did not use a full BTE solution or consider the graphene selection rule.

[31] S. Tamura, Phys. Rev. B **27**, 858 (1983).